The leopard never changes its spots: realistic pigmentation pattern formation by coupling tissue growth with reaction-diffusion

Supplementary material

Marcelo de Gomensoro Malheiros*
Computer Science Center
FURG, Brazil

Henrique Fensterseifer†
Institute of Informatics
UFRGS, Brazil

Marcelo Walter‡
Institute of Informatics
UFRGS, Brazil

1 Overview of parameters

The pattern generated by our technique depends on several parameters, either related to the model or to its simulation (that is, the discrete numerical integration of the model equations).

The model parameters are, from the most to the least important:

- r, the ratio of diffusion rates between reagents A and B, which gives the overall structure of the pattern;
- s, the overall pattern scale, which affects the visual size of pattern features;
- U_a, the upper bound for the A concentration (defaults to unbounded), which is important for establishing the effect of saturation, thus breaking the wavelength of the pattern features;
- L_b, the lower bound for B concentration, which must be zero for typical Turing patterns, or positive for altering the pattern structure (defaults to zero);
- U_b, the upper bound for the B concentration (defaults to unbounded), sometimes used to further change local pattern dynamics, usually having a value close to U_a; and
- L_a, the lower bound for A concentration, kept as zero for all experiments shown.

For simplicity, we enforce the bounds given by U_a, U_b, L_a and L_b within the integration loop. However, those bounds are conceptually part of the model itself. As outlined in our paper, these values can be incorporated into the differential equations by adding rational terms and reducing the time step.

For the simulation parameters, we have the following, again from the most to the least important:

- the initial domain resolution, discretized into a rectangular matrix of m rows and n columns;
- the boundary conditions, either a toroidal wrap-around or a non-flux boundary;
- the growth rate, specifying the time interval between matrix expansion operations;
- the total duration of the simulation;
- the random seed for the random number generator used, defaulting to 1;
- the amplitude of the local random production added to the current concentration of B (when needed), provided that the sum is below U_b;

*e-mail: mgmalheiros@gmail.com
†e-mail: rique.hf@gmail.com
‡e-mail: marcelo.walter@inf.ufrgs.br

- the initial constant concentration for A, with the constraint of being in the (L_a, U_a) interval, defaulting to 4;
- the initial constant concentration for B, with the constraint of being in the (L_b, U_b) interval, defaulting to 4;
- the amplitude of the random variation added to the initial concentration of B, provided that the sum is below U_b, defaulting to 1; and
- Δt, the time step used for the numerical forward Euler integration, defaulting to 0.01.

2 Generating pattern variations

It should be noticed that the pattern variation is induced by three parts of the simulation. First, by the initial random concentrations of B. Then, by the random choice of row and column indices during the matrix expansion operations. Finally, and when needed, by the random localized production of B along a row of the domain matrix, as described in the neural crest experiments.

In Figure S1 we illustrate the effect of just altering the random seed, using the same parameters from the reticulate whipray experiment.

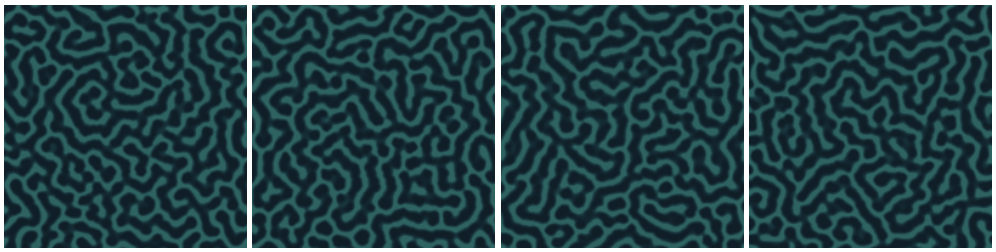

Figure S1: Effect of distinct random seeds for reticulate whipray experiment shown in Figure 9.

From this same experiment, we may also change just the ratio parameter, as shown in Figure S2, or both the ratio and the lower bound for B, as in Figure S3. Those modifications can be viewed as analogous to the parametric variations provided by the distinct technique of noise-based procedural texturing.

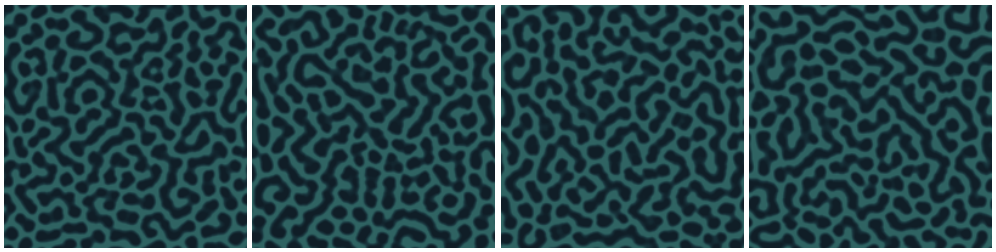

Figure S2: Effect of making $r = 12$, with the same seeds as in Figure S1.

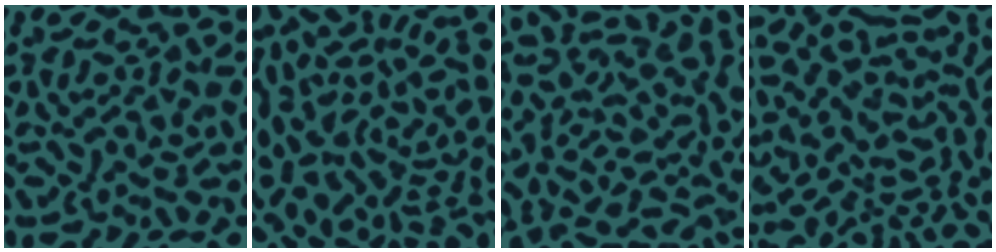

Figure S3: Effect of making $r = 12$ and $L_b = 3$, with the same seeds as in Figure S1.

In Figure S4 we illustrate again the change of only the random seed, but now with the same parameters from the honeycomb whipray experiment.

Figure S4: Effect of distinct random seeds for honeycomb whipray experiment shown in Figure 10.

Following this last experiment, we may also change just the ratio parameter, as shown in Figure S5, or only the lower bound for B, as in Figure S6.

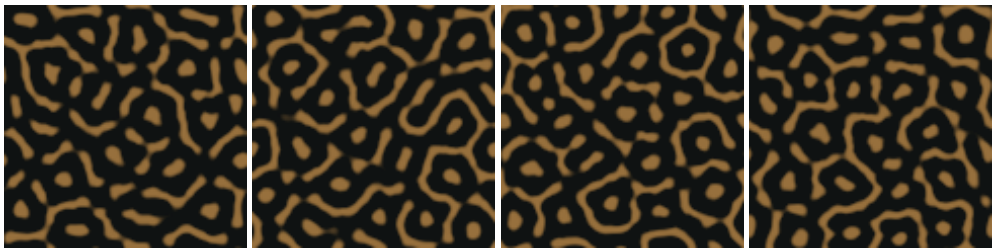

Figure S5: Effect of making $r = 5$, with the same seeds as in Figure S4.

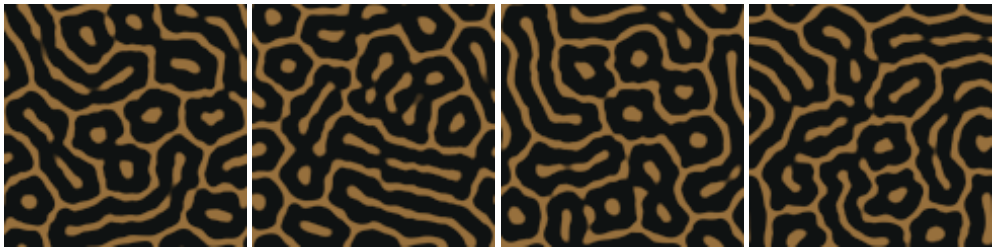

Figure S6: Effect of $L_b = 1$, with the same seeds as in Figure S4.

3 Exploratory procedure

As explained in our paper, the implementation is geared to interactive experimentation, therefore we have systematically explored variations of the parameter set, focusing first on mapping the overall patterns possible, and then manually adjusting parameters to match a particular desired pattern (whether possible at all).

In this section, we give a brief overview of our exploration of the parameter space to determine whether we could accurately simulate patterns from the broad *Dendrobates* genus of poison dart frogs. The several species of this genus present colorful skins, mixed with round and blob-like black spots.

The initial step was to locate interesting ranges for both the ratio r and the upper bound U_a parameters, as the usage of "saturation" is known to yield large and constant-valued pattern regions. In Figure S7 we show a parameter map built by continuously varying the r parameter on the horizontal axis while also varying U_a in the vertical axis. Note that patterns typically do not form with ratios below 4, and the useful range of values for the upper bound for A depends on each specific ratio. We did not apply growth at this time.

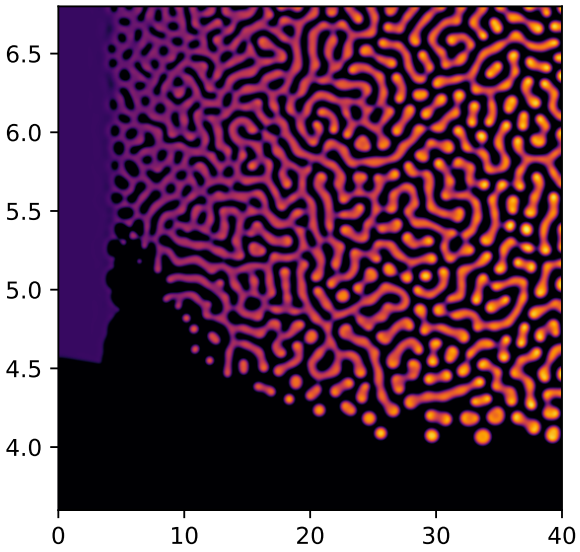

Figure S7: Parameter map built by continuously varying the r parameter, from 0 (left) to 40 (right), and varying U_a from 3.6 (bottom) to 6.8 (top). The domain is static and with size 512 by 512, with $\Delta t = 0.001$. Simulation took 15,000 iterations.

By examining in Figure S7 the areas that produced features shaped like spots and blobs, we selected a smaller parameter space where $r \in [4, 10]$ and $U_a \in [5.5, 6.8]$. To cover this smaller region, several pattern mosaics were generated in batch from these two intervals.

Differently from Figure S7, which is a single image resulting from one simulation with continuous parameter variation, a mosaic is a collection of independent simulations, where each image is the outcome of a single simulation with fixed parameters. Mosaics are more flexible for tuning parameters, because it is harder to spot subtle differences caused by slight parameter variations in a large continuous parameter map. One such mosaic is shown in Figure S8, picking a few values for r in the interval $[4.5, 6.5]$, and some other values for U_a in the interval $[6.2, 6.8]$. Each domain has also growth applied, where the same growth rate is used for every pattern in the mosaic.

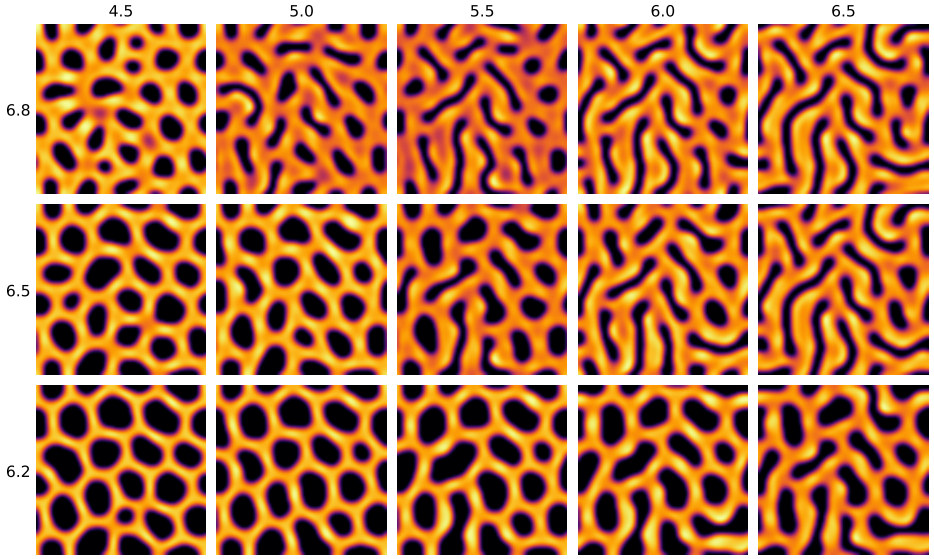

Figure S8: Pattern mosaic for $r \in \{4.5, 5.0, 5.5, 6.0, 6.5\}$ (columns) and $U_a \in \{6.2, 6.5, 6.8\}$ (rows). The growth rate is 0.5 expansions per second and $\Delta t = 0.01$, lasting 5,000 iterations. The initial size is 50 by 50 and the final size is 75 by 75. Each image is a distinct simulation, where the same pair of r and U_a values are used.

At first we tried to match the specific pattern of the blue poison dart frog (*Dendrobates tinctorius "azureus"*). As shown in Figure S9, even among individuals of the same species the pattern details vary greatly, albeit maintaining the overall pattern structure.

Figure S9: Blue poison dart frogs (*Dendrobates tinctorius "azureus"*). Left: photo by H. Zell (Wikimedia Commons, CC BY-SA 3.0). Right: photo by Cliff (Flickr, CC BY 2.0).

Following visual similarity, we have then selected as a candidate a particular simulation from Figure S8 (left column, middle row) with parameters $r = 4.5$ and $U_a = 6.5$. Running this simulation again with a large domain and by applying a simple blue-to-black color map, we produced the pattern shown in Figure S10.

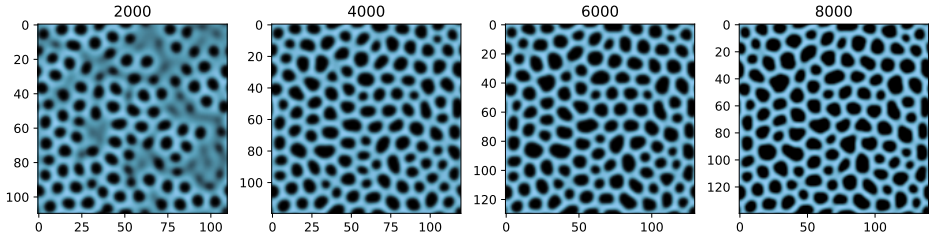

Figure S10: First pattern development for blue poison dart frog, with initial size 100 by 100 and final size 140 by 140, $r = 4.5$, $s = 2$, $U_a = 6.5$, growth rate 0.5 per second and $\Delta t = 0.01$. The axes indicate the matrix dimensions. The respective iteration count is shown on top of each image, as the simulation proceeds.

Further refinement was made exploring variations of other parameters, like setting values for U_b close to U_a. One of the interesting results found is shown in Figure S11, demonstrating that by explicitly setting an upper limit for B we generate further increasing dark blobs, similar to one of the frogs in Figure S9. The development sequences of Figures S10 and S11 help illustrate that even intermediate results may match particular frog patterns. Therefore, another important choice made at this point is to adjust the length of the simulation, on a case-by-case basis.

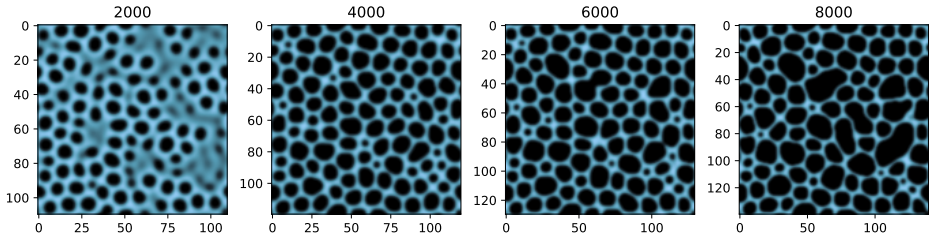

Figure S11: Second pattern development for blue poison dart frog, with the same patterns as in Figure S10, plus setting $U_b = 6.0$.

We opted to go further and then address a more complicated pattern. We sought to validate a formation hypothesis for the distinct and wide black stripes of the yellow-banded poison dart frog (*Dendrobates leucomelas*), as discussed in our paper. The initial phase would be a reaction-diffusion simulation in a static and thin domain, yielding a set of black and yellow stripes, as shown in Figure S12. This was the prepattern for the second phase.

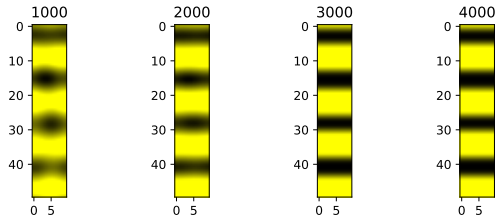

Figure S12: First phase for yellow-banded poison dart frog experiment. The domain is static, with size 50 by 10 and parameters $r = 4.5$, $s = 4$, $U_a = 6.8$, $U_b = 6.2$ and $\Delta t = 0.01$,

We then would fine-tune several of the parameters for a second phase, slightly varying r, U_a, U_b and growth rates based on the parameters of Figure S12. A few of the experiments made are shown in Figure S13. The visually best match then resulted in Figure 11 of our paper.

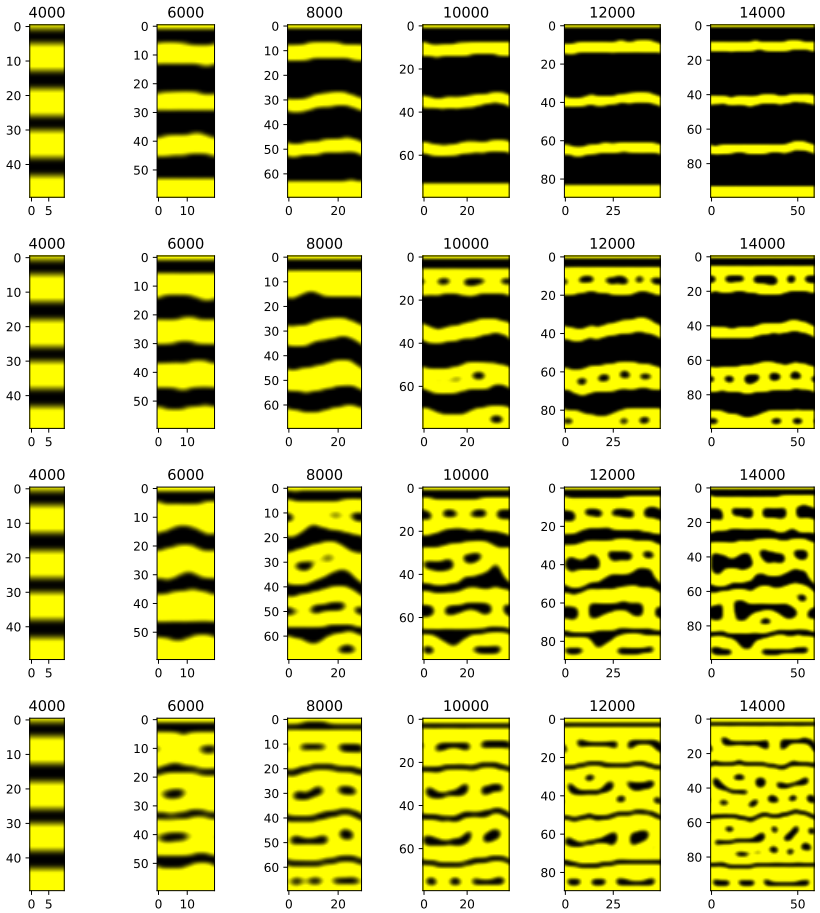

Figure S13: Variations of Figure S11, with initial size 50 by 10 and final size 125 by 85, $r = 4.5$, $s = 2$, growth rate 0.5 per second and $\Delta t = 0.01$. We have also $U_a = 6.6$ and $U_b = 6.3$ (first row), $U_a = 6.7$ and $U_b = 6.3$ (second row), $U_a = 6.7$ and $U_b = 6.7$ (third row), $U_a = 6.9$ and $U_b = 6.5$ (fourth row).

We used mainly Figure S7 as a starting point, but have also employed another large continuous parameter map charting the variation of r against L_b, which yields yet another kind of base pattern for values of $r \geq 20$ and $L_b \geq 2$, as shown in Figure S14. Here, no upper bounds are enforced. The leopard pattern, particularly, was developed by having $r = 40$ and $L_b = 2$.

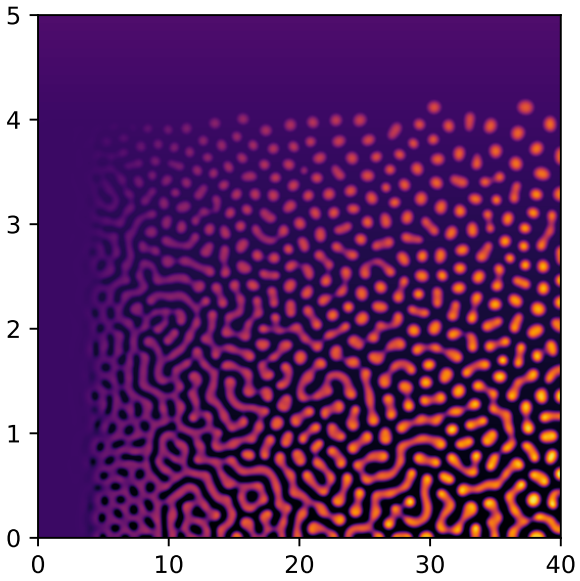

Figure S14: Another parameter map, built by continuously varying the r parameter, from 0 (left) to 40 (right), and varying L_b from 0 (bottom) to 5 (top). There are no upper bounds imposed to A or B. The domain is static and with size 512 by 512, with $\Delta t = 0.001$. Simulation took 15,000 iterations.

4 Interpolation as an approximation for growth

In this section, we show the outcome of using image interpolation, as discussed in Section 8.2, instead of our proposed matrix expansion scheme. We run the same simulations as in our paper but with bicubic image interpolation applied at the same discrete domain growth rate.

It is interesting to notice that interpolated expansion seems to still produce intricate patterns given an initial prepattern with enough detail already present, as in Figures S15 and S16. The results are also visually smoother than the experiments shown in Figures 9 and 10 from our paper.

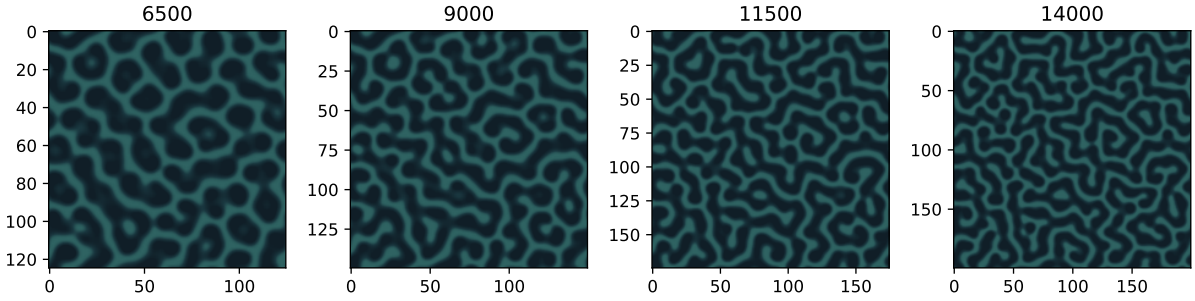

Figure S15: Image interpolation applied to the experiment shown in Figure 9.

On the other side, the randomness added through approximate cell division with the matrix expansion scheme seems to be fundamental to the appearance of pattern discontinuities, which then develop into the marking features of yellow-banded poison dart frog (already shown), squirrel (Figure S17) and leopard (Figure S18) patterns. For the leopard pattern is also of

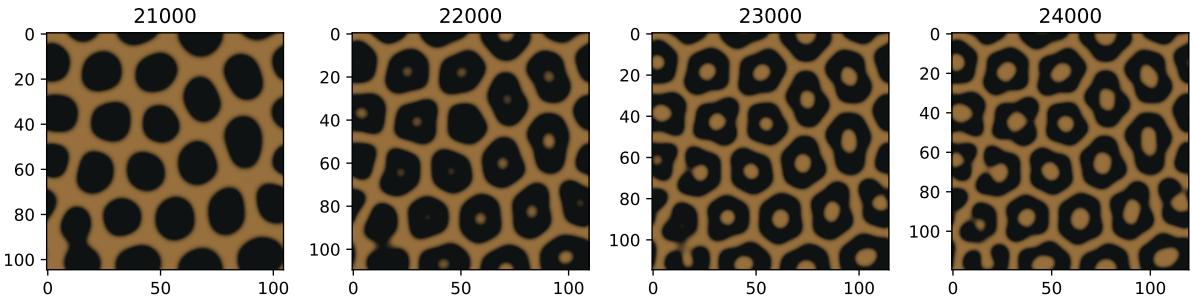

Figure S16: Image interpolation applied to the experiment shown in Figure 10.

notice that spots perfectly arranged into a hexagonal lattice yield symmetric hexagonal rosettes, while unorganized spots still develop into familiar irregular rosettes.

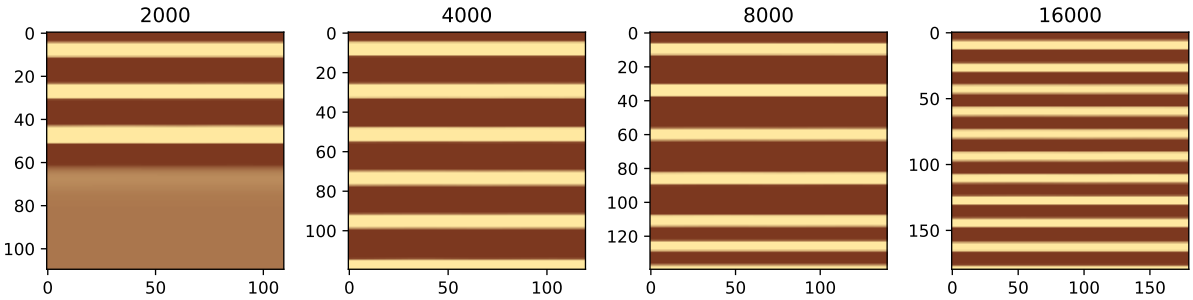

Figure S17: Image interpolation applied to the experiment shown in Figure 12.

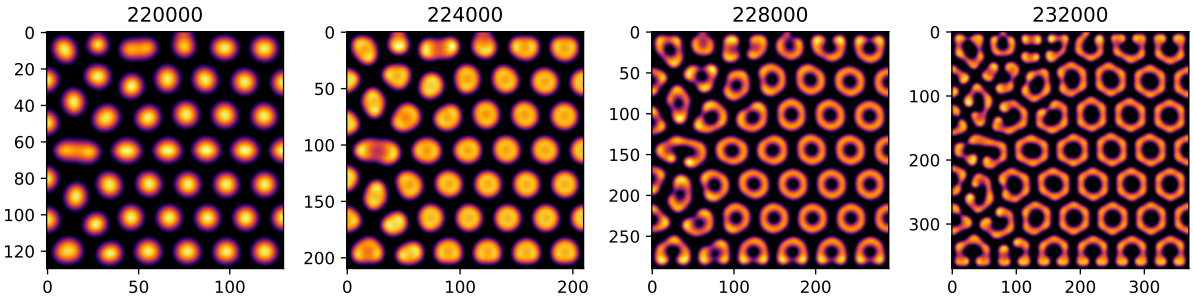

Figure S18: Image interpolation applied to the experiment shown in Figure 15.